Histone-DNA assemblies in archaea : shaping the genome on the edge of life

Henneman, B.

CHAPTER 4

Mechanical and structural properties of archaeal hypernucleosomes

This chapter is based on:

Bram Henneman*, Thomas Brouwer*, Clara van Emmerik, Ramon A. van der Valk, Mandy Erkelens, Monika Timmer, Nancy Kirolos, Hugo van Ingen, John van Noort & Remus T. Dame. *Mechanical and structural properties of archaeal hypernucleosomes*. Submitted.

* These authors contributed equally

Abstract

Many archaeal species express homologues of eukaryotic histones H3, H4, H2A and H2B, which organize the genome and play a key role in gene regulation. The structure and function of archaeal histone-DNA complexes remain largely unclear. Recent X-ray crystallography studies of *Methanothermus fervidus* histone HMfB bound to DNA fragments shows formation of hypernucleosomes consisting of DNA wrapped around an 'endless' histone-protein core. Such a structure is in line with observations suggesting that histone-DNA complexes consisting of an integer number of dimeric units of archaeal histones are formed *in vivo*. However, whether such a hypernucleosome structure assembles on a long DNA substrate and which interactions provide for its stability, remained unclear.

Here we describe micromanipulation studies of complexes of the *M. fervidus* histones HMfA and HMfB in solution. Our experiments show that hypernucleosome assembly results from cooperative binding of histones to DNA, facilitated by stacking interactions between neighboring histone dimers. Furthermore, rotational force spectroscopy demonstrates that the HMfB-DNA complex is left-handed, but that torque can drive it in a right-handed conformation. The structure of the hypernucleosome is thus dependent on stacking interactions and force. Electrostatic interactions facilitate ionic modulation of structural plasticity,

and torsional plasticity allows for absorption of supercoiling. Therefore, stacking interactions, differential behavior of different histones, and force-dependent handedness imply an important role for archaeal histones as transcription regulators, responsive to environmental changes.

Significance statement

Histones play an important role in genome compaction and gene regulation of Eukaryotes. Archaea also express histones, but they lack a key feature of the eukaryotic histone: the N-terminal tail, important in eukaryotic transcription regulation. Archaea are highly relevant as they are one of the main pillars of life, and the role of archaea as a link between the last universal common ancestor in life on earth (LUCA) and Eukaryotes becomes more unequivocal. With no N-terminal tail, archaea must have an alternative way of modulating DNA accessibility. We investigated how archaeal histones compact DNA. Its mechanisms of compaction are suggestive of primordial bacterial-like transcription regulatory mechanisms preceding eukaryotic regulatory mechanisms.

Introduction

Dynamic genome organization is a prerequisite for a compact yet active genome throughout all domains of life. Eukaryotes use histones, which wrap DNA into nucleosomes to compact and functionally organize their genomes. These histones have N-terminal tails that can be post-translationally modified, changing their physico-chemical properties, which is key in defining the functional chromatin state (293). Current views on evolution agree that eukaryotes are part of the branch of archaea, which are single-cellular organisms that share many cellular mechanisms with Eukaryotes (3, 10, 47, 294). Most archaeal species express rudimentary homologues of eukaryotic histones with the characteristic histone fold (13, 177, 295), but lack the N-terminal tail (140, 186, 296-298). In addition to histones, archaea express other small architectural proteins, nucleoid-associated proteins (NAPs). These NAPs are also involved in genome organization and may complement and compete with histones to regulate genes (299, 300).

The prototypical archaeal histones are HMfA and HMfB from *Methanothermus fervidus* (193). HMfA and HMfB are homologues of eukaryotic histones in terms of sequence and structure (140). HMfA and HMfB share 84% sequence identity. These proteins are expressed at varying ratios as a function of growth phase (251). Although estimates of absolute expression levels of individual histones are lacking, HMfA is prevalent during exponential growth (1.5x the amount of HMfB), and present in equal amounts as HMfB during stationary growth (251). This might imply that these proteins have evolved different DNA-binding properties – and correspondingly distinct functions – in the cell. HMfA and HMfB are capable of forming homo- and heterodimers, which subsequently can form larger structures (171, 251, 301, 302). The binding of HMf dimers to DNA results in bends in DNA at low protein concentrations, and has been reported to yield "beads on a string" nucleosome-like structures at higher protein to DNA ratios (193). HMf proteins bind preferentially to intrinsically curved DNA sequences *in vitro* (303). There is currently no evidence of the existence of specific DNA sequence signatures enhancing histone binding *in vivo*, although studies in *Methanothermobacter thermautotrophicus* and *Thermococcus kodakarensis* indicate that histone positioning favors repetitive motifs of AT and GC base pair steps (221). These motifs facilitate the distortion needed for DNA wrapping. Systematic evolution of ligands by exponential enrichment (SELEX) experiments have yielded two high affinity DNA-binding sequences for HMfB *in vitro* (164). Binding of HMf proteins to this sequence yields nucleosome-like structures, in which 60 bp of DNA is proposed to be wrapped around a tetrameric protein core composed of two interacting HMf dimers (160). Here, we will refer to the DNA compaction mode

of HMf proteins as wrapping, even when the DNA is wrapped less than one turn. The histone tetramer model is supported by micrococcal nuclease (MNase) digestion studies of chromatin from *Haloferax volcanii*, which yield undigested DNA fragments 60 bp in size (220, 221). However, the histone tetramer model has been challenged by the results of similar studies in *T. kodakarensis*, which yield DNA fragments ranging from 30 – 450 bp in 30 bp increments (165). The sizes of these DNA fragments were interpreted as reflecting the existence of histone multimers of varying sizes bound along the genome. A notable recent crystallography study of HMfB on 90 base pair DNA fragments supports the formation of a multimeric histone filament established by interactions between adjacent histone dimers and of wrapping of DNA fragments around an endless protein core, creating a

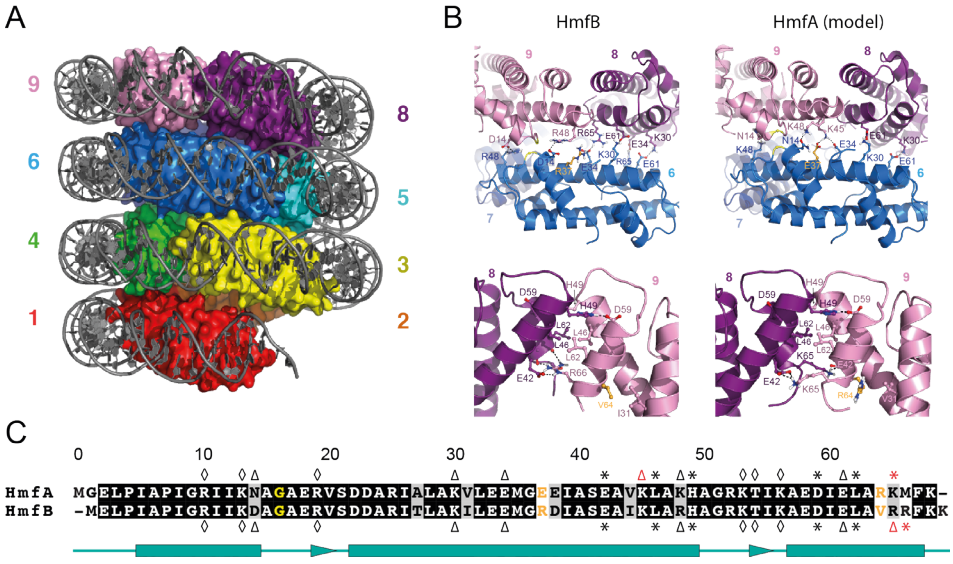

Figure 4.1: The hypernucleosome and *Methanothermus fervidus* histones HMfB and HMfA. A) The HMfB hypernucleosome structure as described by Mattiroli *et al*. (PDB: 5T5K (27)). Figure taken from Henneman *et al*. 2018 with permission (28). B) Hypernucleosome interfaces of HMfB (left; water-refined and starting from the 5T5K structure) and HMfA (right; water-refined and starting from the homology model). Top panels show the stacking interface, bottom panels show the tetramer interface. Interacting residues are labeled; hydrogen bonds are shown by dashed lines. Important residue differences between HMfA and HMfB are colored in orange. The closely packed residues G16 in the stacking interface are shown in yellow spheres (Cα only). C) Sequence alignment of HMfA and HMfB. Conserved residues are shown in black boxes, conservative changes in grey and non-conservative changes in white boxes. Residues are numbered according to HMfB sequence. The two sequences are 84% identical and have 94% similarity. Residues directly contacting the DNA are indicated with diamonds (◊), residues forming the tetramerization interface are marked with asterisks (*) and stacking residues are indicated with triangles (Δ) for HMfA (top) and HMfB (bottom). Differences in interacting residues between HMfA and HMfB are indicated with red symbols. Important residue differences between HMfA and HMfB are colored in orange and G16 residues are shown in yellow, matching panel B.

quasi-continuous superhelix (**FIGURE 4.1A**) (197). This structure is referred to as the hypernucleosome (134). The hypernucleosome is left-handed like the eukaryotic nucleosome, although it has been reported that archaeal histones can accommodate both left- and right-handed wrapping configurations (171, 304, 305). It was proposed that hypernucleosomes are not just held together by interactions between adjacent dimers, but also by stacking interactions between the layers of dimers within the hypernucleosome (**FIGURE 4.1B, C**) (134). The disparate findings from *H. volcanii* and *T. kodakarensis*, as well as the crystal structure, indicate that molecular insights into the role of histones in archaeal chromatin organization are important for understanding archaeal genome compaction.

In this study, we provide direct evidence of hypernucleosome formation in solution and of its capability of transitioning in handedness. The hypernucleosomes formed by HMfA and HMfB homodimers exhibit subtle differences in amino acid composition, resulting in different stacking energies. This underlies different structures of the hypernucleosome, which may be the key to a mechanism for transcription regulation in archaea.

Results

Both HMfA and HMfB cooperatively compact DNA

To determine the degree of DNA compaction by HMfA and HMfB, we performed Tethered Particle Motion experiments (TPM) (195). Here, the Root Mean Squared displacement (RMS) of a bead connected to a surface-attached DNA tether provides a quantitative readout of DNA conformation (FIGURE S4.1A). We investigated the binding of HMfA and HMfB to a 685 bp DNA molecule containing a random, naturally occurring sequence (*see* MATERIALS AND METHODS). We observed an abrupt and drastic reduction in RMS of the DNA tether over a narrow concentration range during titration of both proteins, which indicates that DNA compaction by both HMfA and HMfB is highly cooperative. Such cooperativity is due to either direct protein-protein interactions or facilitated protein-DNA binding through structural effects of adjacently bound HMfA or HMfB proteins (171, 306) (FIGURE 4.2).

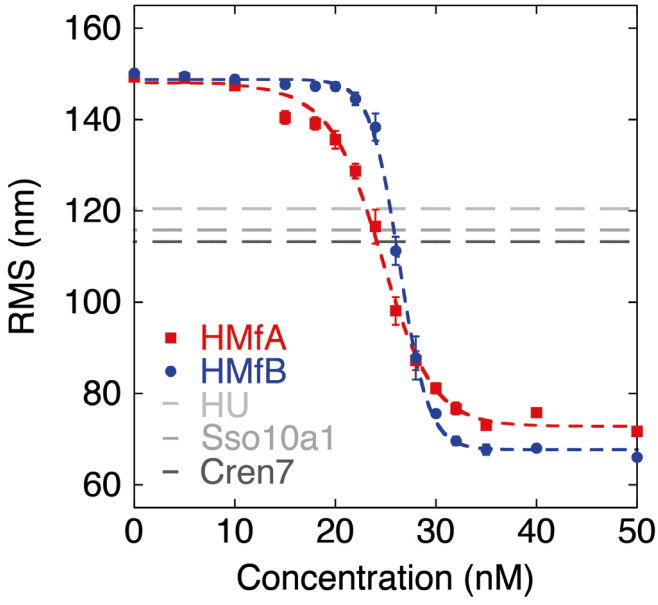

Figure 4.2. Both *Methanothermus fervidus* histone proteins HMfA and HMfB drastically and cooperatively compact DNA in Tethered Particle Motion experiments. Root mean square displacement (RMS) excursion of the bead for HMfA and HMfB on a DNA substrate is shown as a function of protein concentration. Dashed lines are to guide the eye. Error bars indicating the standard error of the data points (N≥100) are mostly hidden behind the data points. In grey, saturation levels of the bacterial NAP HU and archaeal NAPs Sso10a1 and Cren7 – which are known to organize and compact DNA – are indicated, as reported by Driessen *et al.* 2014, Driessen *et al.* 2016 and Driessen *et al.* 2013 (33-35).

As a dimer, HMf proteins bend DNA by partial wrapping to an angle that is similar to those induced by DNA-bending proteins such as the bacterial NAP HU and the archaeal NAPs Cren7 and Sso10a1 (125, 127, 193, 292, 307, 308). These proteins reduce the RMS on a substrate of equal length from 150 to 110-120 nm at saturating protein concentrations (127, 292). A much stronger reduction in RMS down to ~70 nm was observed for HMfB and ~75 nM for HMfA. The extent of this change cannot be explained by DNA bending induced by individual HMfB dimers. The high degree of DNA compaction together with the pronounced binding cooperativity suggests adjacent packing of HMfB (and HMfA) proteins that together wrap DNA. By determining the maximum deflection of the bead in TPM, we found an end-to-end distance of 24 ± 4.7 nm for the HMfB-DNA complex at saturating protein concentrations for this specific DNA substrate (**figure S4.1**). This number agrees with the theoretical end-to-end distance of the hypernucleosomal structure observed in the crystallography studies (197). Both histones bind to DNA in a cooperative manner, with HMfB showing a more pronounced cooperative binding than HMfA. Differences in the stacking interface or tetramerization interface of HMfA and HMfB may underlie the difference in DNA compaction (**figure 4.1B** and **C**).

HMfB organizes long DNA tethers into endless hypernucleosomes

The mechanical stability of the hypernucleosome was investigated by force spectroscopy. HMfB hypernucleosomes were reconstituted *in vitro* on a torsionally unconstrained DNA construct, at 100 nM HMfB, well above the K_D. Hence, we expect full coverage of the DNA. Force spectroscopy revealed a characteristic unfolding response to low-high-low force cycling (**figure 4.3A** and **B**). Binding of HMfB resulted in a large compaction of the DNA. The absence of hysteresis at the low force regime (<50 pN) indicates that the manipulation of the HMfB-DNA complex occurs in thermodynamic equilibrium: stretch-release cycles could be repeated multiple times without qualitative change to the data. The force extension curve of the HMfB-DNA complex shows three regimes of extension (**figure 4.3A**). In regime I, at forces below 1 pN, the force-extension curve features a small extension and high stiffness. In regime II, between 2 and 10 pN, the tether is longer and appears to be less stiff than in regime I. In regime III, at forces above 20 pN, the extension of the complex follows that of bare DNA, which is stiffer than the complex in regime II. Most of the force extension curve of the HMfB-coated DNA could be captured in these three regimes, and we interpret the more horizontal parts as transitions between these regimes.

We modeled the two most extended structures, in force regime II and III, with

the kinked and regular worm-like chains (WLCs), respectively. In regime III the complex followed the force-extension behavior of bare DNA with a persistence length of 50 nm. For regime II, we fitted a persistence length of approximately 4 nm, suggesting a much more flexible tether. The most compacted structure, regime I, could not be modeled by a WLC and shows a linear extension between 0.1 and 2 pN. We used the linear part of a freely-jointed chain (FJC) to describe

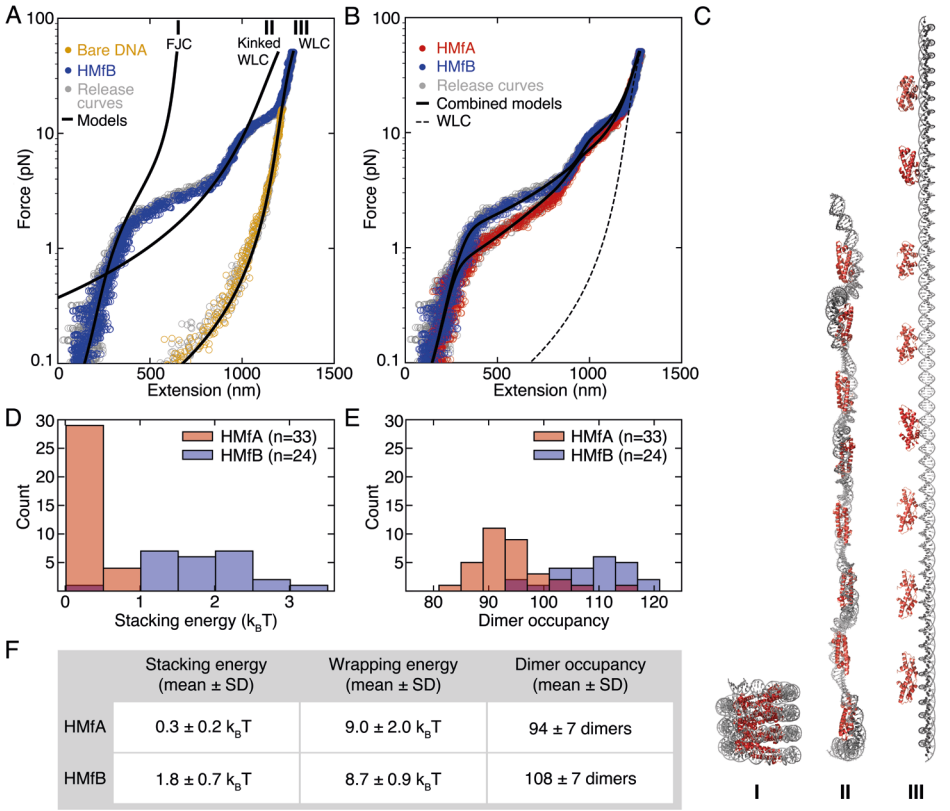

F

	Stacking energy (mean ± SD)	Wrapping energy (mean ± SD)	Dimer occupancy (mean ± SD)
HMfA	0.3 ± 0.2 k_BT	9.0 ± 2.0 k_BT	94 ± 7 dimers
HMfB	1.8 ± 0.7 k_BT	8.7 ± 0.9 k_BT	108 ± 7 dimers

Figure 4.3: Force spectroscopy experiments on the hypernucleosome reveal stronger stacking in HMfB tethers than in HMfA tethers. Red: HMfA; blue: HMfB; yellow: bare DNA. A) Force spectroscopy on a HMfB-DNA complex at 100 nM of HMfB and a bare DNA molecule reveals three levels of compaction. We fitted these to a freely-jointed chain (FJC) (I), kinked worm-like chain (WLC) (II), and WLC (III). The release curves overlapped with the stretch curves, which indicates that HMfB-DNA the stretch-release cycle was in equilibrium. B) Comparison between HMfA hypernucleosomes and HMfB hypernucleosomes. The WLC model for bare DNA was added as a reference (dashed black line). The free energy for dimer stacking and DNA wrapping was extracted by fitting the unfolding model (black lines). C) Cartoons of three states of the HMfB-DNA complex corresponding to the model fit in A, with representative compaction, illustrating the 7-fold compaction of the hypernucleosome compared to bare DNA. D) Histogram of stacking energies of HMfA and HMfB. E) Histogram of occupancy of DNA by HMfA and HMfB dimers. F) Mean stacking energy, wrapping energy and dimer occupancy, with standard deviation (SD).

this regime of the force-extension curve.

The mechanical properties of the complex in these three force regimes suggest three different structures of the tether. Stacking of HMfB dimers into a hypernucleosome would create a relatively stiff structure that can only be stretched to a limited extent without breaking the protein-protein stacking interactions. Based on the crystal structure of the HMfB hypernucleosome (197), we expect a maximal extension of 4 nm per dimer for the most condensed structure (**figure 4.3C, I**). When the stacking interactions are broken due to excessive force, individual dimers may remain bound to the DNA. Such a structure would have a much larger extension per HMfB dimer than the stacked hypernucleosome. If all DNA-protein contacts remain intact, the structure follows a highly curved DNA trajectory (**figure 4.3C, II**). Such curved DNA corresponds to a decrease of the apparent persistence length (285, 309), which is consistent with the observed force-extension relation in regime II. Increasing the force further breaks protein-DNA interactions to yield an unperturbed DNA trajectory (**figure 4.3C, III**), which would have similar mechanical properties as bare DNA. Indeed, at forces larger than 20 pN the force-extension curve overlaps with that of DNA. Thus, the experimental force-extension curves suggest a two-step transition from a hypernucleosome into a fully stretched DNA tether.

For a more quantitative analysis we developed a statistical mechanics model that includes the transitions between the three structures, as described in materials and methods. In analogy with the forced unfolding of eukaryotic chromatin (310), we modeled the entire force-extension curve as a linear combination of the extension of individual dimer-DNA complexes in either of the three states and in addition to a small fraction of bare DNA (*see* **Materials and Methods** for model details). For every dimer that binds to the DNA tether, the extension changes and the free energy is reduced by a binding and/or stacking energy. For each dimer in state II, we imposed a deflection angle of 10 degrees resulting in a reduction of the persistence length as described by Kulić and Schiessel (309). Release curves fully overlap with the stretch curves. The absence of hysteresis in all curves indicates that all transitions are in thermodynamic equilibrium at low forces, allowing an equilibrium model to describe the transitions between the states.

The force-induced transitions between the three states of an HMfB-coated DNA tether are captured by the model (**figure 4.3B**). The first transition (I to II) at 2 pN indicates a low stacking energy of $1.8 \pm 0.7\ k_BT$. The increase in extension is large with ~500 nm, which means that the stacked hypernucleosome is easily disrupted by force (**figure 4.3D**). Unwrapping of the DNA from the dimers at 10

pN takes more energy (8.7 ± 0.9 k_BT), and increases the extension by only ~200 nm. These transitions appear as gradual changes in extension, likely because of the large number of dimers, the small changes in extension and the fast kinetics. We found an average of 108 ± 7 dimers per tether. A footprint of 30 bp per HMfB dimer would allow 121 dimers to bind this DNA molecule. It therefore appears that the DNA molecule is not fully saturated, implicating defects in stacking of the hypernucleosome (**figure 4.3E**). Interestingly, the fitted number of dimers did not change in multiple stretch and release curves of the same hypernucleosome, suggesting that the dimers remain bound to and positioned on the DNA, even at high forces.

TPM experiments showed that HMfB compacts DNA slightly more than HMfA (**figure 4.2**). In force spectroscopy, the force-extension curves for HMfA-DNA complexes were similar to those for HMfB-DNA complexes (**figure 4.3B**), although the transitions between stacked and unstacked states occurred at lower forces, 0.5 rather than 2 pN. Correspondingly, we found a higher stacking energy and dimer occupancy for the HMfB-DNA complex compared to the HMfA-DNA complex, but a similar wrapping energy (**figure 4.3D-F**). The high similarity in stiffness and extension of the complexes at forces below the unstacking transition (I to II) and the similar wrapping energy after unstacking, highlights the universality of the hypernucleosome structure, whereas the difference in stacking energy and occupancy clearly distinguishes the mechanical properties of the protein-DNA filaments formed by the two homologues. This may be biologically relevant as differences in mechanical stability may modulate the balance between gene compaction and accessibility *in vivo*.

Stacking interactions mediate hypernucleosome formation

The basis for stacking of HMfA and HMfB homodimers lies in their primary structure. We analyzed both histones in terms of interaction residues (**figure 4.1C**). Using water refinement with HADDOCK (311) on the HMfB hypernucleosome crystal structure and modeling the HMfA hypernucleosome structure based on that same crystal structure, we were able to identify the possible stacking interactions within the hypernucleosome. For HMfB, we determined interactions between R48-D14, K30-E61 and E34-R65. For HMfA, we found interactions between K31-E62 and E35-K62. In order to investigate whether these interactions indeed mediate hypernucleosome formation, we expressed and purified HMfA stacking mutant $HMfA_{K31A\ E35A}$. We performed TPM experiments similar to those described above. We found that the mutants reduced the RMS to ~78 nm in TPM experiments (**figure 4.4**), which is similar to the values found for $HMfA_{wt}$ on

DNA. However, the concentrations at which this reduction in RMS takes place, is much higher for $HMfA_{K31A\ E35A}$ than for $HMfA_{wt}$. For $HMfA_{wt}$, a K_D of 25 nM is estimated, whereas for $HMfA_{K31A\ E35A}$ the estimated K_D is 750 nM. This indicates that cooperative hypernucleosome formation is strongly dependent on stacking interactions mediated by residues K31 and E35.

Although HMfB has 1 stacking interaction more than HMfA, the stacking interactions of both proteins have a similar number and type of hydrogen bonds. When we calculate the total free energy of all interface residues (stacking interfaces and dimer-dimer interfaces including hydrophobic interactions), we find that HMfA contacts are energetically more stable than HMfB contacts (**FIGURE 4.3F**). Reduced repulsive forces between the HMfA dimers because of the charge swap at position 37 and the lack of positive charge at position 69 also favor a more stable HMfA complex. However, at HMfB position 64, there is a valine that features a hydrophobic interaction with I31, whereas HMfA has an arginine at this position (**FIGURE 4.1C**). The large size of this residue disrupts the hydrophobic interaction. This may make the C-terminal α-helix of HMfA more flexible, leading to a less compact and less stable hypernucleosome. Earlier studies support this interpretation, as a V64R mutation in HMfB leads to reduced electrophoretic mobility of the histone-DNA complex and a slightly impaired nucleosome formation (137, 312, 313).

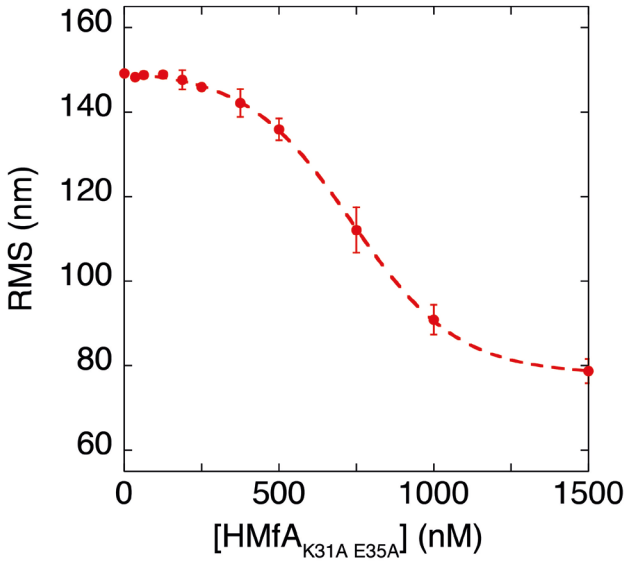

Figure 4.4: Characterization of $HMfA_{K31A\ E35A}$. Root mean square displacement (RMS) excursion of the bead for $HMfA_{K31A\ E35A}$ on a DNA substrate is shown as a function of protein concentration. Dashed lines are to guide the eye. Error bars indicate the standard error of the data points (N≥100). Note that the x-axis is very different compared to **FIGURE 4.2**.

The hypernucleosome forms a left-handed structure on DNA

Wrapping DNA into a hypernucleosome imposes a distinct chirality. To reveal handedness and torsional stiffness of the HMfB hypernucleosome, we used rotational force spectroscopy on a torsionally constrained hypernucleosome. Therefore, the hypernucleosome is unable to release torsional stress by swiveling around the attachment point. The resulting torque would affect the mechanical properties of the hypernucleosome, which we refer to as the HMfB-DNA complex when stretched. We monitored the extension of the hypernucleosome at a constant force, after applying negative (FIGURE 4.5A) and positive (FIGURE 4.5B) twist to a HMfB hypernucleosome.

The unstacking transition of negatively twisted complexes was shifted to higher forces. The force plateau shifted up to 10 pN. Thus, the energy for the unstacking transition is increased: more force is required to unstack the hypernucleosome.

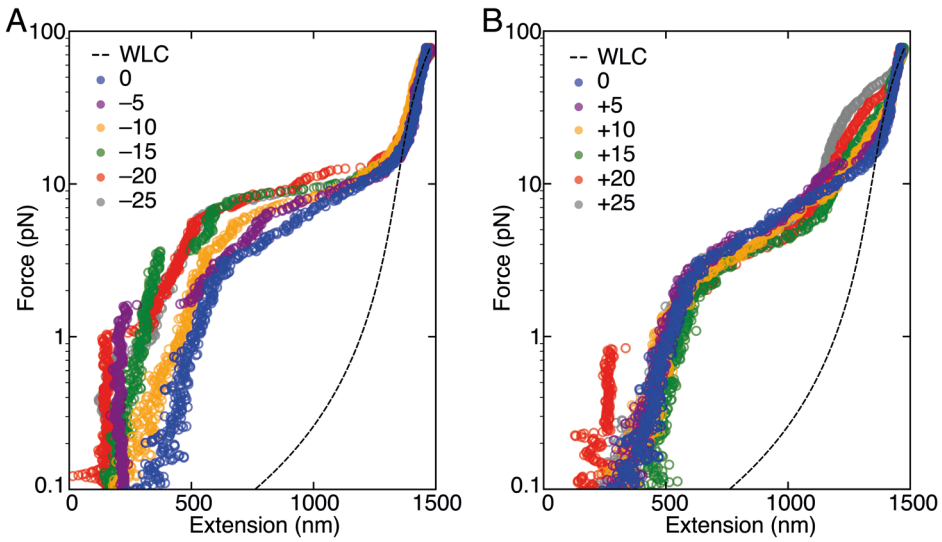

Figure 4.5: Stretching a torsionally constrained HMfB-DNA complex reveals left-handedness of the hypernucleosome, and shows increased affinity of HMfB dimers for positively twisted DNA. A) Negative twist as a result of 5-25 rotations increases the unstacking force of the hypernucleosome. In addition, excess negative twist causes the HMfB-DNA complex to buckle, resulting in a dramatic decrease of its extension. Both observations point to the left-handedness of the hypernucleosome. The unwrapping transition appears largely unaffected, resulting in a continuous decondensation of the tether around 10 pN. B) Positive twist as a result of 5-25 rotations recovers the unstacking plateau. Strikingly, positive twist increases the rupture force of the unwrapping transition of HMfB dimers. An increasing force is necessary to reverse the bending effect of HMfB dimers on DNA. At very low forces the beads appear to stick to the cover slip for certain curves (-5, -20, and +20 rotations, especially).

Large amounts of negative twist further compact the HMfB-DNA complex by buckling the tether complex at forces below 1 pN. The second transition to unbent DNA appeared unaffected by negative twist.

Positive twist on the other hand somewhat extended the range of the unstacking transition to 2-10 pN. Such behavior is a feature characteristic of a left-handed structure, and in agreement with the HMfB-DNA co-crystal structure (197). More strikingly, the second transition between bent and straight DNA is disfavored by positive twist, but not by negative twist. It appears that unstacked HMfB dimers can better accommodate positive twist than bare DNA. The affinity for HMfB dimers increases with the number of twists.

An unstacked HMfB-DNA complex imposes a right-handed structure on DNA

Unfolding a torsionally constrained HMfB-DNA complex builds up torque due to the untwisting of the hypernucleosome (**figure S4.2**). The unstacking transition (between I and II in **figure 4.3A**) of a torsionally constrained hypernucleosome features an increased and more gradual force plateau compared to a torsionally unconstrained hypernucleosome. As a result, the unstacking transition merges with the transition that we attribute to unwrapping DNA from the HMfB dimers (regime II to III in **figure 4.3A**). Since HMfB dimers are likely coupled on the DNA, the unwrapping of one dimer creates torsional stress, which impedes unwrapping of the next dimer, resulting in an anti-cooperative transition.

By maintaining a fixed force larger than the unstacking force of the hypernucleosome, and monitoring the extension under twist, we were able to determine the handedness of the unstacked HMfB-DNA complex (**figure 4.6**). For low forces (f=2.0 pN) either negative or positive twist induced a reduction in extension due to buckling of the complex superstructure. Note that the presence of HMfB-induced bends favors plectonemes over DNA melting, which would occur in bare DNA for negative twist at this force. The asymmetry in twist response in HMfB-decorated tethers only occurs at force above 3 pN. Alternatively, negative twist may unwrap the HMfB dimers, increasing the length of the tether. Similar to bare DNA, positive twist only supercoils the tether. This implies that the unstacked HMfB-DNA complex forms a right-handed superhelix and that the HMfB dimers are stabilized on the DNA by positive torque. The force required to completely unwrap the DNA was correlated with the applied twist. HMfB dimers appeared to have a higher affinity for positively twisted DNA than for negatively twisted or relaxed DNA. This observation is supported by the release curves of the force spectros-

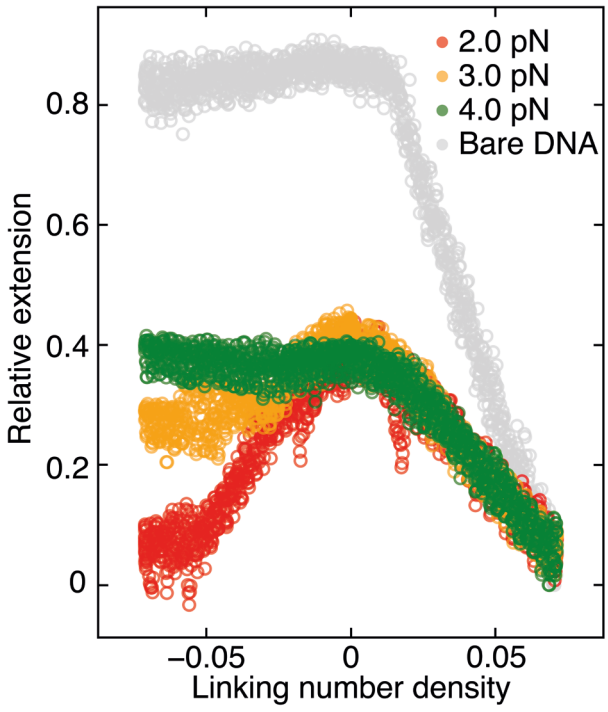

Figure 4.6: Torque stabilizes the hypernucleosome and reveals a right-handed chirality of unstacked HMfB-DNA complexes. A torsionally constrained HMfB hypernucleosome was compacted by twisting the molecule under constant force. At 2.0 pN, both positive and negative twist reduce the extension presumably by buckling. At higher forces, negative twist caused the HMfB dimers to unwrap from the DNA, which induced stretching of the HMfB-DNA complex. These measurements suggest that the unstacked HMfB-DNA complex is right-handed. As a reference, we included a twist-extension curve of bare DNA at 1.0 pN. Note that the slope for the HMfB-DNA complex is much smaller than for bare DNA.

copy experiments (FIGURE S4.3), which show that positively twisted complexes more readily restack into hypernucleosomes than relaxed or negatively twisted DNA.

The slope of the curve beyond the buckling transitions reveals more details of the twisted complex. Bare plectonemic DNA reduces its extension by approximately 40-100 nm per rotation, which depends on force, as the size of the loop at the tip of the plectoneme decreases with force (314). For unstacked HMfB-DNA complexes we measured a reduction of the extension of 16 nm per rotation, much lower than bare DNA, independent of force. This is consistent with a fixed HMfB-induced bend at the tip of the plectoneme, which defines the tip curvature, and thus the geometry of the plectoneme.

Discussion

The hypernucleosome structure may be a key feature of archaeal chromosome compaction. Here we characterized the structural and mechanical properties of the hypernucleosome in solution. We found that hypernucleosomes composed of stacked *M. fervidus* histone homodimers HMfA and HMfB compact DNA much stronger than similar DNA-bending proteins. Both the HMfA- and the HMfB-DNA complexes featured a two-step unfolding mechanism that could be captured quantitatively in the transitions between a hypernucleosome, an array of wrapped dimers that kink the DNA trajectory, and a stretched DNA molecule to which dimers remain bound. HMfB featured a higher stacking energy than HMfA, resulting in a larger occupancy as well as a higher stability of the hypernucleosome against force.

The stiffness of hypernucleosomes is larger than that of stacked eukaryotic nucleosomes (315). This may be explained by the different nature of the stacking interactions. Interactions between eukaryotic nucleosomes are known to be mediated by flexible histone tails. Our data suggests that the archaeal hypernucleosome on the other hand is mediated by stacking interactions between the globular histones that form the hypernucleosome. Stacking energies of HMfA and HMfB dimers (~2 k_BT) are much lower than the 17 k_BT reported for eukaryotic nucleosome stacking (316). The unwrapping of DNA from the HMfA and HMfB dimers also starts at similar forces as the unwrapping of eukaryotic nucleosomes. However, in hypernucleosomes this happens reversibly, whereas nucleosome unwrapping is generally not in equilibrium.

The equilibrium conditions made it possible to capture the entire force-extension curve in a statistical physics model. This worked better for the unstacking transition than for the unwrapping transition. It should be noted though that modelling of the wrapped dimers as kinks in the DNA trajectory might be naive, as the high occupancy of the DNA yields a dimer-dimer distances that are much smaller than the typical deflection length for which the Kulić and Schiessel model is valid (309). Moreover, this model assumes a flat one-dimensional kink, while the super-helical structure of the unfolded hypernucleosome may be more complex. A deflection angle (10°), which matched the curves best, is rather small for the 30 base pair footprint of a HMfA or HMfB dimer. Nevertheless, the resulting force dependent reduction of the end-to-end distance matched quantitatively with the force-extension curve. We resolved a clear transition from a flexible (regime II) to a stiffer WLC (regime III), using the same number of dimers as in the low force transition, indicating that this unfolding intermediate can be effectively modeled

as an array of wrapped dimers.

In the crystal structure, the hypernucleosome compacts DNA in a left-handed manner, which resembles DNA wrapping by eukaryotic histones. In accordance, we found that negative supercoiling stabilizes the most compact regime of the HMfB-DNA complex. However, after breaking the stacking by force a right-handed HMfB-DNA structure was observed. The right-handed HMfB-DNA complex has been described previously as a functional form, responding to environmental cues *in vitro* (251, 305). Depending on conditions, force and torque, a right-handed HMfB-DNA complex may have a biological function in archaea.

The archaeal genome is not only organized by histones but also by other NAPs. The components of the organizational machinery however differ per phylum, class and order. Histones are found in almost every branch of the archaeal domain. Currently, evidence in support of hypernucleosome formation has only been obtained for *M. fervidus* using x-ray crystallography, and for *T. kodakarensis* using MNase digestion of isolated chromatin and analysis of effects of histone binding on transcription *in vivo* (165, 197). It is likely that also histones from other species are able to assemble into hypernucleosomes (134). Formation of a hypernucleosome is likely stochastic, and initiation at multiple sites may lead to lateral frustration. Nevertheless, long stretches of hypernucleosome will probably be rare in the presence of processivity factors driving transcription elongation (317). Also, as nucleosomes are occluded at transcription start sites based on MNase digestion studies, the length of hypernucleosomes may in most cases be limited to a length on the order of genes or operons (172).

The majority of archaeal chromosomes contains genes coding for two or more histones. This may provide archaea with a means to regulate gene expression via changing the length and stability of the hypernucleosome in response to growth phase or environmental cues (251). *M. fervidus* histones form homo- and heterodimers, and, based on sequence similarities, histones from other species may be able to do so as well. This would provide archaea with a wide range of tools for transcription regulation (318). For instance, heterodimers may bind to DNA and interact with other heterodimers via one multimerization site, while other sites remain unbound. Homodimers may form hypernucleosomes, which can be interrupted by other homodimers incapable of certain interactions. Furthermore, sequence specificity in certain histone variants may direct histones to specific genomic targets. The emergence of the N-terminal tail may have diverted the eukaryotic histone from the archaeal histone, eventually resulting in alternative abilities to regulate genes than in archaea (134). The current methods of biological

analysis at the single molecule level allow for detailed, mechanistic measurements that have the potential to shed light on the evolutionary path of genome compaction and transcription regulation.

Materials and Methods

DNA substrate preparation

For the TPM DNA subtrate, a random sequence of 50% GC content (CGGCGCAAATTCGTGACCAGTTGCATCAGCTGCGTGAGCTGT-TTATCGCAGCATCGTAACAGGATAGTGAAGAAGACT) was cloned into pBR322, as described previously (127), resulting in plasmid pRD121. We used PCR to generate and amplify a 685 bp linear substrate (sequence in **SUPPLEMENTARY INFORMATION**) containing the cloned sequence, using digoxygenin- and biotin-labeled oligonucleotides (195).

For magnetic tweezers a 3646 bp DNA fragment based on plasmid pFW01 (pBP-CYC1(wt)/3 derivative (319)) was digested with BsaI and BseYI (New England Biolabs). The fragment was separated using agarose gel electrophoresis and purified using a Promega Wizard® SV Gel and PCR Clean-Up System. It was subsequently labeled with digoxigenin and biotin at either end by a Klenow reaction.

For the torsionally constrained construct, pUC18-based plasmid pTB01, (containing 12 repeats of the Widom 601 sequence (320)), was digested with BsaI and BseYI. The 4092 bp digested product was separated using agarose gel electrophoresis and purified using a Promega Wizard® SV Gel and PCR Clean-Up System. Subsequently, a 650 bp handle containing multiple digoxigenin- or biotin-modified bases was ligated on each end. Details on both approaches are provided elsewhere (321). The 4092 bp substrate based on plasmid pTB01 qualitatively behaved the same as the 3646 bp pFW01-based substrate.

HMfA and HMfB

HMfA and HMfB were kindly provided by John Reeve and Kathleen Sandman (16).

Expression and purification of HMfA mutant

The histone mutant gene was synthesized by GeneArt (Thermo Fisher Scientific, MA) and cloned into pET30b vectors using Gibson assembly. This resulted in plasmids pRD323, expressing $HMfA_{K31A\ E35A}$. pRD323 was transformed to *E. coli* BL21 pLysS (DE3). 1L LB medium with 25 mg/ml chloramphenicol and 50 mg/ml kanamycin was inoculated with 1% v/v culture grown to saturation o/n. The culture was grown at 37°C with shaking at 250 rpm. At $OD_{600} \approx 0.6$, expression of

the mutant was induced with 1 mM IPTG. The culture was grown for 1 h at 37°C with shaking at 250 rpm. Cells were harvested after 1 h and spun down for 30 minutes at 11,325 xg and at 4°C. Cells were resuspended in resuspension buffer (50 mM Tris-HCl pH8, 100 mM NaCl and 5 mM $MgCl_2$ in water), then frozen at -80°C and thawed the next day. DNase I, PMSF and lysozyme were added and cells were lysed using the pressure homogenizer unit 5 (Homogenising Systems Ltd, UK) at 350 MPa in resuspension buffer. The lysate was then centrifuged for 30 minutes at 11,325 xg and at 4°C. Pellets were resuspended in 3M NaCl. The resulting mixture was incubated at 95°C for 10 minutes, then spun down for 20 minutes at 10,967 xg and at 4°C. Treated lysate was desalted using a 5 ml HiTrap desalting column (GE Healthcare, IL) using the Äkta start protein purification system (GE Healthcare, IL) at RT. Flow-through was analyzed using Coomassie-stained SDS-PAGE gels. The fractions containing the proteins of interest were loaded onto a 5 ml HiTrap DEAE Sepharose FF column (GE Healthcare, IL) and eluted with 150 ml 50 mM Tris-HCl pH 8 and a sodium chloride gradient from 0 to 1 M using the Äkta pure chromatography system (GE Healthcare, IL) at RT. Peak fractions of 0.5 ml were collected and checked on Coomassie-stained SDS-PAGE gels. Fractions containing the protein of interest were combined and concentrated to 500 µl using Amicon ultrafiltration membranes (Merck, Germany; cut-off: 3 kDa) at 3700 rpm. The combined fractions were loaded on a Superdex 75 Increase 10/300 GL gel filtration column (GE Healthcare, IL) and eluted with a degased solution of 50 mM Tris-HCl pH 8 and 100 mM NaCl in water, using the Äkta pure chromatography system at RT. Peak fractions of 0.5 ml were collected, checked on Coomassie-stained SDS-PAGE gels and purity was examined using mass spectrometry. Fractions with less than ~5% impurities were considered pure. Concentration of $HMfA_{K31A\ E35A}$ was determined using a Pierce BCA Protein Assay kit (Thermo Fisher Scientific, MA) and was 151.3 µM. Protein solutions were plunge frozen and stored at -80°C.

Tethered Particle Motion

The tethered particle motion experiments were carried out as described previously (322). The measurement buffer contained 50 mM Tris-HCl, pH 7 and 75 mM KCl. We used an anisotropic ratio cut-off of 1.3 and a standard deviation cut-off of 8% to select single-tethered beads. The end-to-end distance of the DNA substrate was determined by taking the average of the extremities (2.5% largest values) of the deflection of 25 beads in the xy plane at 50 nM of HMfB and subtracting the radius of the bead (**FIGURE S4.1**). The end-to-end distance was obtained by triangular calculation.

Force spectroscopy and rotational spectroscopy

HMfA and HMfB were diluted to 100 nM in measurement buffer. 1 pM DNA substrate was introduced in the flow cell and incubated with histones, following the TPM protocol, but using paramagnetic M270 beads (Dynabeads; Thermo Fisher Scientific, USA) instead of polystyrene beads. Details of the force spectroscopy experiments and the multiplexed magnetic tweezers setup have been described elsewhere (321). In each measurement, the force was increased exponentially from 0.01 to 40 pN in 70 seconds, and decreased at the same speed.

Quantitative modeling of stretching the hypernucleosome

To interpret the force-extension behavior of the hypernucleosomes, we developed a statistical mechanics model in collaboration with Thomas Brouwer. HMfA and HMfB dimers bound to the DNA were distributed over three conformations, representing different levels of compaction. In the lowest force regime, HMfA and HMfB homodimers assembled into a hypernucleosome. The extension of the hypernucleosome was modeled by a freely-jointed chain (FJC) (323, 324) (**EQUATION 4.1**),

$$z_{FJC}(f) = L_{dimer}\left(coth\left(\frac{f_b}{k_B T}\right) - \frac{k_B T}{f_b}\right) \tag{4.1}$$

where $z_{FJC}(f)$ is the extension per dimer, b the Kuhn length, f the force, k_B Boltzmann's constant, T the temperature and L_{dimer}, which was fixed at 4 nm, which is the length of the DNA segment that is wrapped around a single dimer. The FJC was chosen for its initial linear increase of extension with force, as observed experimentally. In the final model only the linear part of the FJC i.e. an extension up to 2 nm per dimer mattered, as the dimers unstack at larger forces. For low forces ($f_b \ll k_B T$), the FJC describes a Hookean spring with linear extension, and Kuhn length can be rewritten to include stiffness k of the stacked fiber (**EQUATION 4.2**) (323).

$$b = \frac{3k_B T}{kL_{dimer}} \tag{4.2}$$

The second force regime is characterized as a beads-on-a-string structure. In this structure, DNA wraps onto non-interacting HMfA and HMfB homodimers resulting in moderate compaction of the fiber. The beads-on-a-string structure was modeled as an extensible worm-like chain (WLC) (310, 325) (**EQUATION 4.3**).

$$z_{WLC}(f) = L\left(1 - \frac{1}{2}\sqrt{\frac{k_B T}{fP}} + \frac{f}{S}\right) \tag{4.3}$$

in which $z_{WLC}(f)$ is the extension of protein-DNA complex, L is the contour length of the DNA substrate, S the stretch modulus and P the persistence length. Since the footprint of an HMfB homodimer is 30 bp (326), each transition of a dimer from the hypernucleosome into a beads-on-a-string conformation reduces the contour length of the FJC by L_{dimer} and increases the contour length of the WLC with 30 bp. Moreover, each HMf dimer that bends the DNA reduces the persistence length of DNA to an apparent persistence length P_{app} (309) (**EQUATION 4.4**).

$$P_{app} = \frac{P}{\left(1 + PN^2 8\left[1 - \cos\left(\frac{\alpha}{4}\right)\right]/L\right)^2} \tag{4.4}$$

in which N is the number of dimers in the beads-on-a-string conformation and α is the DNA deflection angle induced by the dimer. In addition we added a small free energy contribution per kink g_{kink} that is proportional to the square root of force and does not exceed 0.01 $k_B T$ (327). The model matched the data best using a deflection angle of 10 degrees, which corresponds roughly to the structure depicted in **FIGURE 4.5B**.

At high forces, the HMfA and HMfB homodimers appeared to remain bound, but do not bend the DNA. Each transition therefore reduces the number of kinks in the DNA, resulting in an increase of the apparent persistence length to that of bare DNA, for which we used P = 50 nm and S = 1000 pN (324, 325, 328).

Many different states j of the fiber can be defined containing different distributions of each of the three dimer conformations i, which can be the hypernucleosome, beads-on-a-string, or straight conformation. The total extension $z_j(f)$ of the tether is a linear combination of the extension of each dimer conformation $z_i(f)$ multiplied by the number of dimers n_i in conformation i (**EQUATION 4.5**).

$$z_j(f) = \sum_i n_i z_i(f) \tag{4.5}$$

The free energy per dimer in the hypernucleosome is given by:

$$g_{FJC} = \int z_{FJC}(f)\mathrm{d}f = L_0 \frac{k_B T}{b}\left(\ln\left(\sinh\left(\frac{fb}{k_B T}\right)\right) - \ln\left(\frac{fb}{k_B T}\right)\right) + g_{stack} + g_{wrap} \tag{4.6}$$

using a protein-protein interaction energy g_{stack} and a protein-DNA interaction energy g_{wrap}. The free energy per dimer in the beads-on-a-string and the straight structure is given by:

$$g_{WLC} = \int z_{WLC}(f)\mathrm{d}f = L\left(-\sqrt{\frac{fk_B T}{P}} + \frac{f^2}{2S}\right) \tag{4.7}$$

optionally complemented by g_{wrap} for the wrapped conformation. In addition, the work W done by the bead corresponds to:

$$W = \int f(z_j)\mathrm{d}z \tag{4.8}$$

The total free energy $G_j(f)$ of a particular tether is the work by the bead minus the sum of the free energy contributions of each dimer with an additional force-dependent free energy contribution for the number of kinks $Ng_{kink}(f)$ (327):

$$G_j(f) = W - \sum_i n_i g_i(f) + Ng_{kink}(f) \tag{4.9}$$

Finally, the force dependent extension of the hypernucleosome is calculated as the Boltzmann-weighted mean extension:

$$< z_{tot}(f) >= \frac{\sum_j z_j(f)\exp(-G_j(f)/k_B T)}{Z} \tag{4.10}$$

with partition function $Z = \sum_j \exp(-G_j(f)/k_B T)$.

Prior to fitting, the z-offset z_0 was determined by fitting the WLC for bare DNA at forces >30 pN. Subsequently, the number of dimers on the DNA was determined based on the maximum compaction of state I and state II (*see also* **FIGURE 4.3C**). The stiffness k of the hypernucleosome was fixed at 1.2 pN/nm which yielded a good fit to the data, and since the hypernucleosome unstacks at a relatively low force fitting this value was problematic. **EQUATION 4.10** was fitted to the data between 0.5 and 55 pN to extract the composition, stacking and energy g_{stack} and wrapping energy g_{wrap} from each curve.

Supplementary information

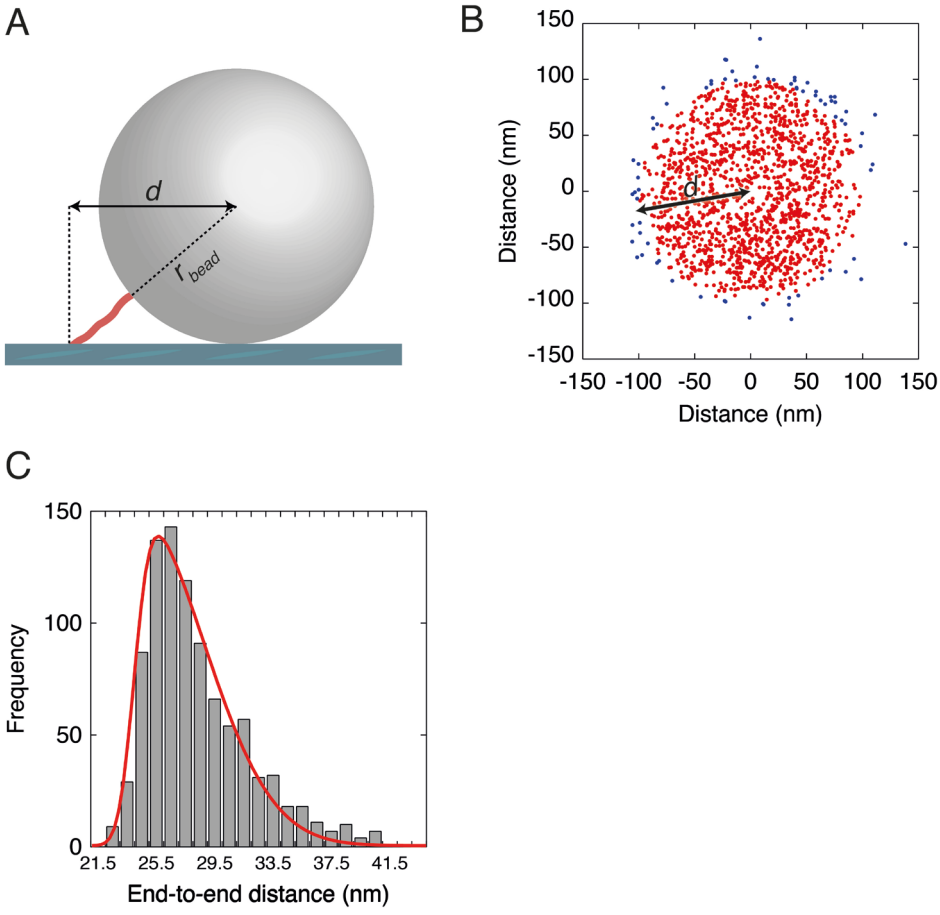

Figure S4.1: End-to-end distance of the HMfB-DNA complex using TPM. A) Schematic of the parameters used in the calculation of the end-to-end distance. *d* is the horizontal distance between the center of the bead and the place where the DNA is attached to the flow cell; r_{bead} is the radius of the bead. B) Positions of TPM bead over 60 seconds at 50 nM HMfB (red and blue). The 2.5% positions at the extremities of the plot (blue) represent the end-to-end distance of the HMfB-DNA complex. C) Skewed Gaussian fit (red) of the end-to-end distance of the 2.5% most distant positions with respect to the center of 25 beads.

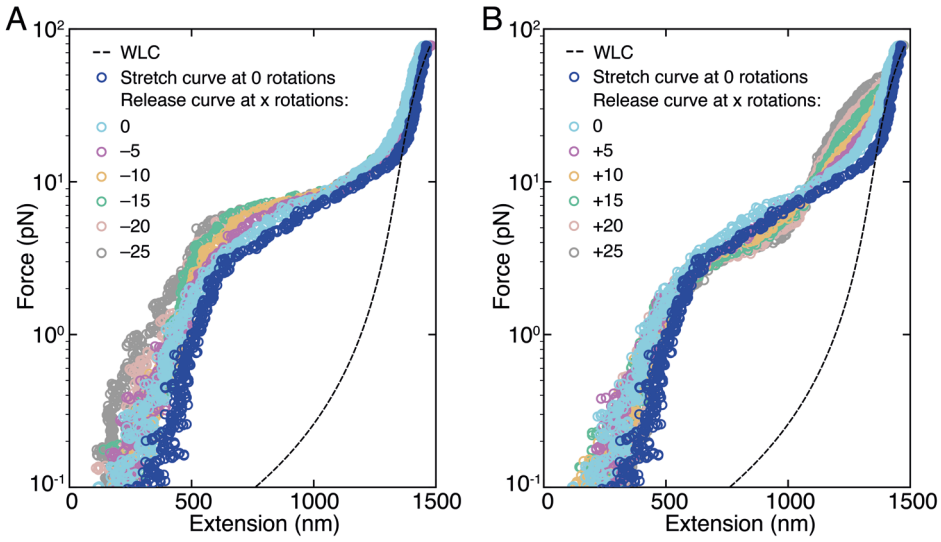

Figure S4.2: Force spectroscopy on torsionally constrained and torsionally free HMfB-DNA complex. At low force (<2 pN) both complexes are identical in length, and the curve overlaps with the freely-jointed chain model (FJC). At high force (>20 pN) the curves overlap with the worm-like chain model (WLC) of bare DNA. In between, the hypernucleosome undergoes an unstacking transition and subsequently an unwrapping transition. Due to the chiral structure of the hypernucleosome, unstacking increases torque, which stabilizes the structure. The torsionally constrained hypernucleosome unstacks at ~10 pN, compared to ~1.5 pN for the torsionally unconstrained hypernucleosome. The unwrapping transition appears unaffected. Fitting the torsionally constrained hypernucleosome yields a higher stacking energy (4.2 ± 0.1 k_BT vs 1.6 ± 0.0 k_BT per dimer), reflecting an increased energy cost for unstacking the hypernucleosome. The wrapping energy is largely unaffected (9.9 ± 0.1 k_BT vs 10.0 ± 0.1 k_BT per dimer). The fit, however deviates somewhat from the data in the transition region. Both molecules are associated with an identical number of HMfB dimers: 103 dimers, from which 95 are stacked in a hypernucleosome. The force extension curves of both molecules converge to a WLC with a contour length of 3646 bp at forces >30 pN.

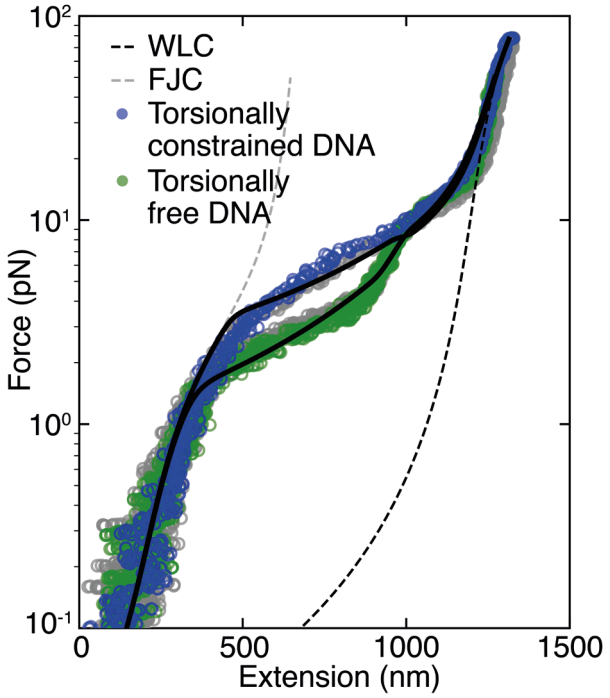

Figure S4.3: Release curves of torsionally constrained HMfB-DNA complexes. A) Force spectroscopy on negatively twisted HMfB-DNA complexes. The release curves suggest that overstretched DNA has higher affinity for HMfB dimers compared to relaxed DNA, shown by the reduced extension of the release curve. As a reference, the stretch curve for 0 twist has been added in bright blue. Upon negative twist, this hysteresis becomes less. B) Force spectroscopy experiments on positively twisted HMfB-DNA complexes. At forces between 10 and 40 pN the extension is reduced with increasing twist, which was also observed in the pulling curve.

DNA substrates

TPM substrate

5’ TTACTTTCACCAGCGTTTCTGGGTGAGCAAAAACAGGAAGGCAAAATGCCGCAAAAAAGG-
GAATAAGGGCGACACGGAAATGTTGAATACTCATACTCTTCCTTTTTCAATATTATTGAAGCAT-
TTATCAGGGTTATTGTCTCATGAGCGGATACATATTTGAATGTATTTAGAAAAATAAACAAATAG-
GGGTTCCGCGCACATTTCCCCGAAAAGTGCCACCTGACGTCTAAGAAACCATTATTATCATGA-
CATTAACCTATAAAAATAGGCGTATCACGAGGCCCTTTCGTCTTCAAGAATTCCGGCGCAAAT-
TCGTGACCAGTTGCATCAGCTGCGTGAGCTGTTTATCGCAGCATCGTAACAGGATAGTGAA-
GAAGACTAAGCTTTAATGCGGTAGTTTATCACAGTTAAATTGCTAACGCAGTCAGGCACCGTG-
TATGAAATCTAACAATGCGCTCATCGTCATCCTCGGCACCGTCACCCTGGATGCTGTAGGCATA-
GGCTTGGTTATGCCGGTACTGCCGGGCCTCTTGCGGGATATCGTCCATTCCGACAGCATCGCCAGT-
CACTATGGCGTGCTGCTAGCGCTATATGCGTTGATGCAATTTCTATGCGCACCCGTTCTCGGAG-
CACTGTCCGACCGCTTTGGCCGCCGCCCAGTCCTGCTCGCTTCGCTACTTGG 3’